OPEN

Endothelial Cell–Specific Inactivation of TSPAN12 (Tetraspanin 12) Reveals Pathological Consequences of Barrier Defects in an Otherwise Intact Vasculature

Chi Zhang,* Maria B. Lai,* Michelle G. Pedler, Verity Johnson, Ralf H. Adams, J. Mark Petrash, Zhe Chen, Harald J. Junge

Objective—Blood-CNS (central nervous system) barrier defects are implicated in retinopathies, neurodegenerative diseases, stroke, and epilepsy, yet, the pathological mechanisms downstream of barrier defects remain incompletely understood. Blood-retina barrier (BRB) formation and retinal angiogenesis require β-catenin signaling induced by the ligand norrin (NDP [Norrie disease protein]), the receptor FZD4 (frizzled 4), coreceptor LRP5 (low-density lipoprotein receptor-like protein 5), and the tetraspanin TSPAN12 (tetraspanin 12). Impaired NDP/FZD4 signaling causes familial exudative vitreoretinopathy, which may lead to blindness. This study seeked to define cell type-specific functions of TSPAN12 in the retina.

Approach and Results—A loxP-flanked *Tspan12* allele was generated and recombined in endothelial cells using a tamoxifen-inducible Cdh5-CreERT2 driver. Resulting phenotypes were documented using confocal microscopy. RNA-Seq, histopathologic analysis, and electroretinogram were performed on retinas of aged mice. We show that TSPAN12 functions in endothelial cells to promote vascular morphogenesis and BRB formation in developing mice and BRB maintenance in adult mice. Early loss of TSPAN12 in endothelial cells causes lack of intraretinal capillaries and increased VE-cadherin (CDH5 [cadherin5 aka VE-cadherin]) expression, consistent with premature vascular quiescence. Late loss of TSPAN12 strongly impairs BRB maintenance without affecting vascular morphogenesis, pericyte coverage, or perfusion. Long-term BRB defects are associated with immunoglobulin extravasation, complement deposition, cystoid edema, and impaired b-wave in electroretinograms. RNA-sequencing reveals transcriptional responses to the perturbation of the BRB, including genes involved in vascular basement membrane alterations in diabetic retinopathy.

Conclusions—This study establishes mice with late endothelial cell–specific loss of *Tspan12* as a model to study pathological consequences of BRB impairment in an otherwise intact vasculature.

Visual Overview—An online visual overview is available for this article. **(*Arterioscler Thromb Vasc Biol*. 2018;38:2691-2705. DOI: 10.1161/ATVBAHA.118.311689.)**

Key Words: blood-brain barrier ■ diabetic retinopathy ■ edema ■ endothelial cells ■ inflammation

Blood-CNS (central nervous system) barrier defects are implicated in retinal and neurological disease. Retinal vascular diseases associated with dysregulated angiogenesis and impaired inner blood-retina barrier (BRB), for example, diabetic retinopathy (DR), are a leading cause of blindness,[1–3] yet, the pathological consequences of barrier defects have been difficult to untangle from other vascular defects. Dysregulated angiogenesis and exudation are also encountered in familial exudative vitreoretinopathy and Norrie disease,[4,5] which are caused by impaired NDP (Norrie disease protein)/FZD4 (frizzled 4) signaling.[6] About 50% of familial exudative vitreoretinopathy cases are because of mutations in the genes encoding the ligand NDP, the receptor FZD4, LRP5 (low-density lipoprotein receptor-like protein 5, a coreceptor), or the coactivator TSPAN12 (tetraspanin 12).[4,5,7,8] Tetraspanin membrane proteins function in diverse biological processes and are linked to human diseases, including cancer, retinal dystrophies, viral infections, and mental retardation.[9] Tetraspanins engage in networks of direct and indirect protein-protein interactions, yet, the molecular basis for their biological activity is incompletely understood.[10,11]

Received on: July 31, 2018; final version accepted on: September 7, 2018.

From the Department of Molecular, Cellular, and Developmental Biology, University of Colorado, Boulder (C.Z., M.B.L., V.J., Z.C., H.J.J.); Department of Ophthalmology, University of Colorado School of Medicine, Aurora (M.G.P., J.M.P.); and Department of Tissue Morphogenesis, Max Planck Institute for Molecular Biomedicine, Faculty of Medicine, University of Münster, Germany (R.H.A.).

Current address for Verity Johnson: ArcherDx, Boulder, CO.

*These authors contributed equally to this article.

The online-only Data Supplement is available with this article at https://www.ahajournals.org/doi/suppl/10.1161/ATVBAHA.118.311689.

Correspondence to Harald Junge, PhD, Department of Molecular, Cellular, and Developmental Biology, University of Colorado, 347 UCB, Room B359b, Boulder, CO 80309. Email harald.junge@colorado.edu

Nonstandard Abbreviations and Acronyms

BRB	blood-retina barrier
CDH5	cadherin5 aka VE-cadherin
COL4	collagen IV
DR	diabetic retinopathy
EC	endothelial cell
ECM	extracellular matrix
FITC	fluorescein isothiocyanate
FZD4	frizzled 4
LRP5	low-density lipoprotein receptor-related protein 5
MC	mural cell
MFAP	microfibrillar-associated protein
NDP	Norrie disease protein
PCR	polymerase chain reaction
PDGFβ	platelet-derived growth factor β
PECAM	platelet endothelial cell adhesion molecule
PKC	protein kinase C
PLVAP	plasmalemma vesicle-associated protein
S1P	sphingosine-1-phosphate
TGF	transforming growth factor
TSPAN12	tetraspanin 12
VE	vascular endothelial
VEGF	vascular endothelial growth factor

FZD4, LRP5, and TSPAN12 form a receptor complex for NDP,[12] and each component of the complex is cointernalized during NDP-induced endocytosis of the receptor complex.[13] We recently proposed that TSPAN12 is an NDP coreceptor that stabilizes the NDP/FZD4 interaction and enhances ligand selectivity of FZD4.[14] A clear prediction of our model is that TSPAN12 functions in the same retinal cell type as FZD4 and LRP5, that is, in endothelial cells (ECs).[15,16]

The role of canonical signaling in pathological vascular growth has been studied in models of retinopathies.[17–19] In addition, NDP has also been studied in neuroprotection,[20] regulation of tumor stroma,[21] and regulation of neural progenitors.[22] However, little is known about the role of NDP/FZD4 signaling in the mature vasculature.

Blood-CNS barrier formation in several developing CNS structures are induced by NDP, WNT7A, or WNT7B ligands,[23–27] and β-catenin is a required mediator of signaling in ECs.[27–29] Among the genes regulated by NDP/FZD4 signaling are regulators of vascular permeability and blood-CNS barrier function, for example, the fenestration component PLVAP (plasmalemma vesicle-associated protein, which is repressed by NDP/FZD4 signaling), the tight junction component Claudin-5, transporters that mediate selective transport into or out of the CNS, and transcription factors, including Sox (SRY-related HMG-box) F family members.[15,27,30–33] However, whether BRB defects downstream of impaired NDP/FZD4 signaling cause retinal pathology, remains unknown.

Ndp, Fzd4, Lrp5, and *Tspan12* gene-disrupted mice show strong vascular morphogenesis defects, including lack of intraretinal capillaries and glomeruloid vascular malformations.[12,17,26,34,35] How NDP/FZD4 signaling mediates retinal angiogenesis, especially intraretinal capillary development, and how Wnt signaling mediates angiogenesis in the forebrain and ventral spinal cord[24,25,27,28,36–43] is not well understood.

Mouse models characterized by an impaired BRB have been developed for the purpose of studying DR. Models based on impaired PDGFβ (platelet-derived growth factor β) signaling[44–48] or hyperglycemia[49] each exhibit compound pathologies that include loss of pericytes, perfusion defects, and hypoxia next to an impaired BRB. Thus, an animal model with normal vascular density, normal perfusion, normal pericyte coverage, yet strong BRB defects, is highly desirable to identify pathological consequences of BRB defects per se.

Here, we report that early EC-specific inactivation of the *Tspan12* gene recapitulates phenotypes observed in *Ndp*, *Fzd4*, and *Lrp5* mutant mice, consistent with a role of TSPAN12 in the NDP receptor complex.[14] Late-induced recombination of *Tspan12* bypasses vascular morphogenesis defects but reveals essential roles in BRB maintenance. Aged mice with long-term BRB defects display immunoglobulin accumulation in the retina, activation of antibody effector systems, cystoid edema, basement membrane alterations, and impaired electroretinogram. Thus, we reveal pathological mechanisms downstream of blood-CNS barrier defects in an otherwise intact vasculature.

Materials and Methods

Data and Material Disclosure Statement

The data and study materials will be made available to other researchers for purposes of reproducing the results or replicating the procedure, pending material transfer agreement. RNA-Seq data have been deposited at NCBI Geo under accession GSE113878.

Animals

All animal work was done in accordance to the Association for Research in Vision and Ophthalmology statement for the Use of Animals in Ophthalmic and Vision Research and with approval from the Institutional Animal Care and Use Committee at the University of Colorado. Animals of both genders were used for all studies. The following Cre-driver lines were used: Tg(Cdh5-cre/ERT2)1Rha,[50] Pdgfrb(BAC)–CreERT2,[51] and Rx-Cre,[52] the latter kindly provided by Drs Eric Swindell and Milan Jamrich. mT/mG reporter mice were obtained from Jackson Laboratories. Conditional knockout mice were generated by first breeding *Tspan12*$^{+/-}$ mice with each Cre-driver line (heterozygous for the transgene), then breeding *Tspan12*$^{+/-}$; *Cre*$^{+}$ mice with *Tspan12*$^{flox/flox}$ mice. The alleles *Tspan12*^{flox} (*Tspan12*$^{tm1.1Hjug}$) and *Tspan12*$^{-}$ (*Tspan12*$^{tm1.2Hjug}$) were generated by gene targeting as described below.

Gene Targeting

The targeting construct for generating a *Tspan12* floxed allele, pTspan12-LFNFL, contained the following sequence segments: exon3 (encoding the start codon and major portions of the first transmembrane segment) was flanked on the 3' end by a loxP site, and on the 5' end by an FRT-flanked PGK-neo-bGH cassette (for positive selection of ES cells) and the 5' loxP site. The 5' homology arm (left arm) consisted of 2978 bp sequence containing exon1, exon2, and adjacent sequences. The 3' homologous arm (right arm) consisted of 2510 bp of intronic sequences downstream of exon3. The construct contained a thymidine kinase cassette outside the homology arms for negative selection of ES cells. The linearized construct was electroporated into EC7.1 ES cells and subjected to negative/positive selection with ganciclovir and G418, respectively. ES cell clones were screened using genomic polymerase chain reaction (PCRs) that amplified the right and left arms separately, using primers outside the left or outside the right homology arms, each combined with a primer inside the

targeting cassette. In addition, the entire targeted region was amplified using primers outside each homology arm. PCR products were further analyzed by restriction digest. A karyotyped ES cell clone (D11) was injected in to C57/BL6 blastocysts, and chimeras with germline transmission were identified by PCR. The FRT-flanked PGKneo cassette was removed by Flp recombination in the germline using FLPo mice, and recombined offspring was identified by PCR. A global knockout allele was generated by recombination of the loxP-flanked exon3 in the germline, using EIIa-Cre. The knockout allele was genotyped using mTSPAN12_LA_fw oligo (5'-GTCTCAAGGGCCATGCCACTG-3') and mTSPAN12_RA_rev oligo (5'-ACTAGCGGTTCCCGAGTAGTCTGTC-3'), yielding a 256 bp amplicon on the knockout allele and a 717 bp amplicon on the wild-type allele. The floxed conditional allele was genotyped using mTSPAN12_LA_fw oligo (above) and TSP12ex3-rev oligo (5'- CCACATTCTACTGGTCCAGGCAGAG-3'), yielding a 403 bp amplicon on the floxed allele and a 301 bp amplicon on the wild-type allele. Mice were backcrossed on a C57BL/6J background.

Preparation and Administration of Tamoxifen

Tamoxifen (Sigma T5648) solutions were freshly prepared at 1 mg/mL in sterile corn oil (Sigma C8267) the day before each injection using a nutator to facilitate dissolution overnight at RT. Solutions were sterile filtered before injection. Fifty microliters of 1 mg/mL tamoxifen in corn oil was administrated by intraperitoneal injection at P1, P2, and P3 for analysis at P7 or P16. For analysis of late-induced adult mice, 100 µL of 20 mg/mL tamoxifen in corn oil was administered in 4 IP injections spaced 2 days apart, starting at P28.

Immunofluorescent Staining

Retinas were processed and stained as described.[53] The following primary antibodies and lectins were used for this study: GS Isolectin B4 Alexa-488 conjugate 1:100 (Invitrogen, I21411), rat PECAM (platelet endothelial cell adhesion molecule) 1:50 (BD, 550274), rat PLVAP 1:50 (BD, 550563), rabbit desmin 1:200 (Cell Signaling, D93F5), rat vascular endothelial (VE)-cadherin 1:100 (BD, clone 11D4), rat complement component C4 1:200 (Cedarlane, CL7504AP), goat transferrin 1:200 (R&D, AF3987), rabbit COL4 (collagen IV) 1:200 (Abcam, 6586), goat albumin 1:200 (Bethyl, A90-234A), goat IBA1 1:200 (Novus, NB100-1028), rat F4/80 1:200 (AbD Serotec, MCA497R), rabbit PKC (protein kinase C) α 1:200 (Santa Cruz, C-20), and rabbit Sox9 1:200 (Millipore, AB5535). IgG was detected using Alexa555-coupled goat anti-mouse secondary antibody (Invitrogen). Other secondary antibodies were Alexa coupled (488, 555, and 647) and directed against rabbit, mouse, or rat (Invitrogen). Fluorescence was visualized using a Nikon A1 confocal laser scanning system or a Leica DM IL epifluorescent microscope.

Branched DNA In Situ Hybridization

Twelve micrometer retinal sections at the level of the optic nerve head were collected. The assay was performed according to manufacturer instructions (QuantiGene ViewRNA ISH Tissue 1-Plex Assay Kit, Affymetrix). The branched DNA probe set was from Affymetrix (m*TSPAN12*: VB-16328) and was used at a 1:50 dilution. Immunostaining was performed subsequent to in situ hybridization.

Quantification of Pericyte Coverage

Confocal images were processed using the ImageJ colocalization plugin. Colocalization of desmin and PECAM was determined and normalized by the PECAM signal. Four images per retina and 3 to 4 retinas per genotype were analyzed.

Retinal Lysates

Two retinas from an P8-10 animal were dissected in cold PBS and homogenized in a 2 mL tube with 0.3 mL lysis buffer (150 mmol/L NaCl, 50 mmol/L Tris pH 8.0, 1 mmol/L CaCl2, 1% NP40, 0.1% N-dodecyl-β-D-maltoside, 3 mmol/L $MgCl_2$, and DNAseI 80 units/mL (Roche), 1× complete ultra EDTA-free protease inhibitor cocktail [Roche]) using an electrical homogenizer (Omni). Proteins were extracted for 40 minutes on ice with gentle shaking. Cell debris and unsolubilized material were removed by 20 000×*g* centrifugation at 4°C for 30 minutes. One hundred four microliter supernatant, 40 µL 4× LDS (Nupage), and 16 µL 1 mol/L dithiothreitol were combined and incubated at 70°C for 10 minutes. Forty microliters of the sample were loaded per lane. VE-cadherin was detected using Millipore anti-VE-cadherin clone Vli37 (MABT886) at 1:1000. PECAM (cell signaling, 77699) and β-actin (Novus, NB600-501H) were probed as loading control.

Fluorescein Isothiocyanate-Dextran Perfusion

Mice were anesthetized with Ketamine/Xylazine 150/10 mg/kg. Unresponsive mice were perfused through the left ventricle with 2 mL of PBS containing 500 units of heparin (Millipore), followed by 10 mL PBS containing 1.5 mg/mL fluorescein isothiocyanate (FITC) conjugated Dextran (500 kDa, Sigma). Perfused retinas were then immediately immersion-fixed and stained as described.[53]

RNA-Sequencing

Seven-month-old mice (tamoxifen at P28) were used to extract total RNA from 4 retinas per genotype (8 samples). DNA was digested (Turbo DNAse free, Ambion), and RNA was ribodepleted (Ribozero RNA removal kit, Illumina). RNA integrity numbers were >8. Library preparation and sequencing were performed at the CU Anschutz Microarray and Genomics Core. Libraries were prepared using the Illumina TruSeq Stranded Total RNA Library Prep Kit (RS-122–2202), and 300 bp fragments were isolated. High output 150 bp paired-end sequencing was performed on 1 lane of an Illumina HighSeq4000 instrument, resulting in 38 to 50 mio reads per sample. The following barcodes were used: 1L_WT1, ATTACTCG; 1R_WT2, TCCGGAGA; 5L_WT3, CGCTCATT; 5R_WT4, GAGATTCC; 10L_CKO1, ATTCAGAA; 10R_CKO2, GAATTCGT; 17L_CKO3, CTGAAGCT; and 17R_CKO4, TAATGCGC. The average reads/bases quality was at least 93% ≥Q30. Reads were mapped against mouse genome GRCm38.p4 C57BL6J using the DNASTAR (version 15) Seqman NGen RNA-Seq module. Among the most highly expressed genes were photoreceptor genes (eg, rhodopsin RPKM [reads per kilobase million] 7034 in wild type). Genes expressed in ECs or microglia were expressed at lower levels (eg, IBA-1/Aif1 RPKM 0.3). Differential gene expression analysis, filtering of genes of interest, and statistical tests were performed in the Arraystar module. Multiple testing correction within the set of 45802 coding and noncoding features was performed with Arraystar moderated *t* test with Benjamini-Hochberg false discovery rate determination. A list of protein-coding genes was created by filtering genes with RPKM ≥1- and ≥2.5-fold change or RPKM ≥0.3- and ≥10-fold change. These gene sets were combined and filtered for $P \leq 0.05$. Nonprotein coding genes were removed. The resulting gene list was subjected to gene ontology analyses in Arraystar (using MGI mouse GO terms) and in the DAVID resource. A list of selected genes of interest is shown in the Table. The processed data file showing the expression of all genes and the raw data files are available at NCBI Geo under accession GSE113878. Filenames ending on R1 indicate 5' to 3' reads, 3' to 5' reads were designated R2.

Electroretinogram

All animals were dark-adapted overnight. Electroretinograms were acquired under red light. Eyes were dilated with 0.5% tropicamide (Akron) and 2% phenylephrine (Paragon BioTeck) and then anesthetized with 90 mg/kg ketamine and 10 mg/kg xylazine (both VetOne). Just before electroretinogram was performed a drop of 2.5 % hypromellose ophthalmic demulcent solution (Akron) was placed onto the cornea. Electroretinograms were performed on a Celeris instrument (Diagnosys). The electrodes were placed onto the cornea, and an impedance of <5 KΩ was ascertained before a combined dark and light protocol (Diagnosys Espion software) was

Table. Differentially Expressed Genes in RNA-Seq Analysis of Four 6-Month-Old Control Versus 4 *Tspan12* ECKO Retinas

Gene Symbol	Description	ECKO RPKM	WT RPKM	Fold change	*P* Value
Antibody effector systems					
C1qa	Complement component 1, q subcomponent, α-polypeptide	9.55	3.18	3.01	0.0000509
C1qb	Complement component 1, q subcomponent, β-polypeptide	10.56	3.16	3.34	0.000162
C1qc	Complement component 1, q subcomponent, C chain	5.66	1.58	3.58	0.000454
C3ar1	Complement component 3a receptor 1, C3a anaphylatoxin chemotactic receptor	0.41	0.04	10.97	0.00144
C4b	Complement component 4B (Chido blood group)	4.63	0.57	8.13	0.00121
Fcgr2b	Fc receptor, IgG, low-affinity IIb	1.16	0.15	7.99	0.000696
Fcgr3	Fc receptor, IgG, low-affinity III	3.01	0.75	4.02	0.000557
Fcer1g	Fc receptor, IgE, high-affinity I, γ-polypeptide	3.17	0.88	3.59	0.00329
Serping1	Serine (or cysteine) peptidase inhibitor, clade G, member 1; C1 inhibitor	8.12	2.23	3.64	0.000298
Chemokines					
Ccl12	Chemokine (C-C motif) ligand 12, C-C motif chemokine 12	1.41	0.01	127.35	0.0189
Cxcl10	Chemokine (C-X-C motif) ligand 10, C-X-C motif chemokine 10	0.75	0.11	6.69	0.00116
Immune process, other					
Adgre1	Adhesion G protein-coupled receptor E1 (F4/80)	0.42	0.09	4.87	0.00152
Cd68	CD68 antigen	7.97	2.51	3.18	0.00106
Cd74	Invariant polypeptide of major histocompatibility complex, class II antigen-associated	1.34	0.18	7.64	0.00793
Cst7	Cystatin F (leukocystatin), Cystatin F	0.51	0	187.28	0.00684
Endou	Endonuclease, polyU-specific; Poly(U)-specific endoribonuclease	1.23	0.46	2.66	0.0019
Edn2	Endothelin 2	1.41	0.12	12.26	0.000222
Egr1	Early growth response 1	37.45	10.18	3.68	0.000254
Fcrls	Fc receptor-like S	0.77	0.03	30.26	0.0332
H2-Aa	Histocompatibility 2, class II antigen A, α	0.6	0.01	58.45	0.0367
Lgals3	Lectin, galactose binding, soluble 3	1.4	0.38	3.7	0.0103
Lilrb4a	Leukocyte immunoglobulin-like receptor, subfamily B, member 4A	0.31	0.02	14.32	0.0606
Mrc1	Mannose receptor, C type 1; Macrophage mannose receptor 1	0.35	0.01	56.97	0.0142
Ms4a6d	Membrane-spanning 4-domains, subfamily A, member 6D	0.3	0	95.43	0.0173
Osmr	Oncostatin M receptor	5.66	2.05	2.76	0.000408
Psmb8	Proteasome subunit β type-8	1.52	0.55	2.78	0.0313
Ppp1r14b	Protein phosphatase 1 regulatory subunit 14B	1.11	0.44	2.53	0.0271
Rgcc	Regulator of cell cycle, Regulator of cell cycle RGCC	1.36	0.47	2.92	0.0201
2610528A11Rik	RIKEN cDNA 2610528A11 gene	15.24	4.98	3.06	0.00353
Slfn8	Schlafen 8, Protein Slfn8	0.5	0.02	25.77	0.0274
Tnfrsf1a	Tumor necrosis factor receptor superfamily, member 1a	2.68	0.97	2.77	0.00913
Trem2	Triggering receptor expressed on myeloid cells 2	2.03	0.5	4.08	0.0196
Extracellular matrix organization and remodeling					
Dcn	Decorin	1.43	0.36	3.98	0.0246
Fbln1	Fibulin 1	2.04	0.2	10.15	0.0408
Fmod	Fibromodulin	1.3	0.46	2.83	0.0279
Lad1	Ladinin	1.78	0.61	2.92	0.00734
Lgals3	Lectin, galactose binding, soluble 3	1.4	0.38	3.7	0.0103
Mfap2	Microfibrillar-associated protein 2	3.46	1.34	2.58	0.0148
Mfap4	Microfibrillar-associated protein 4	1.3	0.11	11.88	0.0134

(*Continued*)

Table. Continued

Gene Symbol	Description	ECKO RPKM	WT RPKM	Fold change	*P* Value
Optc	Opticin	4.42	0.68	6.49	0.00598
Vcan	Versican, Versican core protein	1.98	0.68	2.94	0.0233
Antioxidant activity					
Gpx3	Glutathione peroxidase 3	28.45	5.23	5.44	0.00581
Mgst1	Microsomal glutathione S-transferase 1	3.22	1.12	2.86	0.000985
Sod3	Superoxide dismutase 3, extracellular; extracellular superoxide dismutase	1.87	0.68	2.74	0.0423
Transport					
Slc13a4	Solute carrier family 13 (sodium/sulfate symporters), member 4; protein Slc13a4	2.04	0.35	5.77	0.0139
Ttr	Transthyretin	10.94	3.55	3.08	0.0138
Trf	Transferrin	43.54	14.71	2.96	0.000207
Other					
A2m	α-2-macroglobulin	5.59	1.17	4.79	0.000307
Ankrd7	Ankyrin repeat domain 7	0.52	1.45	0.36	0.000498
Crybb1	Crystallin, β B1	0.58	0	190.01	0.008
Gfap	Glial fibrillary acidic protein	16.83	3.22	5.23	0.00033
Rtkn2	Rhotekin 2, Rhotekin-2	0.42	4.77	0.09	0.00000626
Ptgds	Prostaglandin D2 synthase (brain)	29.09	11.35	2.56	0.001

Selected genes are alphabetically ordered within each biological process heading. Multiple testing correction within the set of 45802 coding and noncoding features was performed with Arraystar moderated *t* test with Benjamini-Hochberg FDR determination, none of the listed genes reached $q<0.05$. FDR indicates false discovery rate; RPKM, reads per kilobase million; and WT, wild type.

run. A- and b-wave amplitudes were determined under scotopic conditions (1 cd s/m^2). B-wave amplitudes were also determined under photopic conditions (10 cd s/m^2).

Software

Nikon NIS-Elements, ImageJ, DNASTAR Lasergene Genomics Suite V15, GraphPad Prism, Microsoft Office 2016, and Adobe Photoshop/Illustrator CS6 were used for data analysis and figure preparation.

Statistics

For comparison of 2 groups, a Shapiro-Wilk test for normality was performed to determine if a parametric or nonparametric test was appropriate. If data passed the normality test, an F test for equality of variances and a 2-tailed, unpaired heteroscedastic or homoscedastic Student *t* test was performed. Where normalized data are presented, individual values were divided by the average of the control group before statistical analysis. For one data set in the electroretinogram panel (indicated in the figure legends) a nonparametric Mann-Whitney *U* test was performed. RNA-Seq data were analyzed for significance of differential gene expression using Arraystar statistics tool, which performs an unpaired, 2-tailed, equal variance Student *t* test. For multiple group comparison, a parametric test was performed using GraphPad Prism by 1-way ANOVA with Tukey post hoc.

Results

Tspan12 mRNA Is Detected in Capillaries and the Neural Retina

To define which retinal cell types express TSPAN12, we localized *Tspan12* mRNA using a branched DNA (bDNA) signal amplification in situ hybridization assay.[54] *Tspan12* message was detected in the retinal vasculature, as well as in the ganglion cell layer and inner nuclear layer, whereas control sections showed no signal after amplification (Figure 1A and 1B). Several other bDNA probe sets that were processed in parallel for a separate study showed distinct and specific staining patterns.[53]

BRB Defects in *Tspan12*$^{-/-}$ Mice

To determine the cell type(s) in which TSPAN12 functions and to examine the role of TSPAN12 in the mature retina, we generated a LoxP-flanked allele (MGI allele symbol *Tspan12*$^{tm1.1Hjug}$, in the following *Tspan12*^{flox}), in which the critical exon 3 (containing the start codon and major portions of the first transmembrane segment) can be removed by Cre-mediated recombination (Figure 1C through 1E). To confirm that recombination indeed results in *Tspan12* gene inactivation, we used EIIa-Cre to induce recombination in the germline, which generated conventional homozygous *Tspan12*$^{tm1.2Hjug}$ mice (in the following *Tspan12*$^{-/-}$). Confocal depth projections of IB4-stained P16 retinas showed glomeruloid vascular malformations and a lack of intraretinal capillaries (Figure 1F and 1G), as reported for a previously generated null mutant.[12] Similar phenotypes have also been described in studies using *Ndp*, *Fzd4*, and *Lrp5* mutant mice (introduction).

BRB defects in *Tspan12*$^{-/-}$ mice would be expected given the role of NDP/FZD4 signaling in BRB induction. Indeed, we detected massive IgG extravasation into the surrounding tissue in mutant retinas (Figure 1F and 1G). Furthermore, these strong BRB defects were associated with upregulation of the EC fenestration component PLVAP (Figure 1H and 1I), especially in veins.

Large Vessel Defects and Increased VE-Cadherin Expression in *Tspan12*$^{-/-}$ Mice

During this analysis, additional large vessel defects became apparent. The number of large vessels in P6-7 retinas was significantly increased in *Tspan12*$^{-/-}$ retinas (Figure IA and IB in the online-only Data Supplement), and aberrant arterial-venous crossings were observed (Figure IC and ID in the online-only Data Supplement). Both types of large vessel defects likely reflect impaired remodeling of the immature vascular plexus. Thus, consistent with previous reports on the role of NDP/FZD4 signaling in the retinal vasculature,[15,26,55] we find that global *Tspan12* inactivation results in BRB defects and abnormal arterial-venous crossings. The VEC-specific adhesion molecule CDH5 (cadherin5 [aka VE-cadherin]) is a core regulator of EC behavior, including vascular integrity and quiescence. We found that the adhesion molecule is upregulated in ECs of P6 *Tspan12*$^{-/-}$ retinas. Quantification of immunofluorescence staining intensity (Figure 2A through 2C) and immunoblot VE-cadherin band intensity from total retina lysates (Figure 2D and 2E) showed that VE-cadherin is about 2.5-fold more abundant in mutant retinas than in wild type. The upregulation of the mediator of vascular quiescence correlates with sluggish sprouting angiogenesis and large vessel defects in *Tspan12* mutant mice. This finding provides novel insights into how impaired NDP/FZD4 signaling and defective angiogenesis are linked.

Tspan12 Functions in Retinal VECs

Next, we used Cdh5(PAC)-CreERT2,[50] Pdgfrb(BAC)–CreERT2,[51] and Rx-Cre[52] to examine the role of TSPAN12 in ECs, mural cells (MCs), and cells derived from retinal precursors, respectively. Because *Tspan12*$^{+/-}$ heterozygotes show no substantial BRB or vascular morphogenesis defects (Figure 1F), we used *Tspan12*$^{flox/-}$ mice positive for the respective Cre transgene, which facilitates removing TSPAN12 activity below the required levels. *Tspan12*$^{flox/-}$, Cdh5(PAC)-CreERT2 mice (ie, *Tspan12* ECKO) displayed prominent BRB defects, lack of intraretinal capillaries, glomeruloid vascular malformations, and upregulated PLVAP expression (Figure 3A through 3E). In contrast, neither BRB defects nor vascular morphogenesis defects were detected in *Tspan12*$^{flox/-}$; Rx-Cre (Figure 3F and 3G) or *Tspan12*$^{flox/-}$; Pdgfrb(BAC)-CreERT2 mice (Figure 3H and 3I). Thus, TSPAN12 exerts angiogenic activity in ECs, the same cell type in which FZD4 and LRP5 are required.[15,16] This finding is consistent with a role of TSPAN12 as coreceptor in the NDP receptor complex.[14]

Reduced MC Coverage in *Tspan12*$^{-/-}$ Mice and *Tspan12* ECKO Mice

Reduced MC coverage has been described as a consequence of impaired vascular β-catenin signaling[15] and MCs are required for BRB formation.[56] The intermediate filament desmin is a marker for pericytes and, to a lesser extent, other MC populations. Wild-type P7 mice showed a high coverage of small and larger blood vessels with desmin-positive cells; only few areas showed a lower degree of coverage (Figure IIA in the online-only Data Supplement). In contrast, P7 *Tspan12*$^{-/-}$ mice showed multiple areas with complete absence of desmin-positive cells (Figure IB in the online-only Data Supplement). Quantification showed that MC coverage was reduced 31% (Figure IIC in the online-only Data Supplement). Analysis of P7 retinas after EC-specific *Tspan12* inactivation (tamoxifen injection between P1 and P3) revealed non-cell autonomous MC coverage defects, which, however, were milder than in global *Tspan12* knockout mice (Figure IID through IIF in the online-only Data Supplement). Examination of *Tspan12*$^{flox/-}$, Pdgfrb(BAC)-CreERT2 retinas and respective controls yielded no evidence for a cell-autonomous role of TSPAN12 in MCs (Figure IIG through III in the online-only Data Supplement). Experiments with mT/mG reporter mice showed that each Cre driver was efficient in inducing recombination (Figure III in the online-only Data Supplement).

TSPAN12 Is Required for BRB Maintenance but Is Dispensable for Vascular Maintenance or MC Coverage

We induced EC-specific inactivation of *Tspan12* in ECs at P28 and analyzed the mice 1 and 6 months later. Massive IgG extravasation was detected at time points both 1 month and 6 months after recombination (Figure 4A through 4D). Confocal analysis of retinas at the 6-month post-recombination time point showed that all 3 retinal vascular layers were normally formed (Figure 4C and 4D). Coverage with desmin-positive cells was normal 6 months after EC-specific recombination in juvenile mice (Figure 4E through 4G), and retinas of either genotype were well-perfused with 500 kDa FITC-dextran via the transcardial route (Figure 4H and 4I). Therefore, late-induced recombination bypassed vascular morphogenesis and MC coverage defects, revealed a role for TSPAN12 in BRB maintenance, and provided a model to study pathological consequences of BRB defects in an otherwise intact vasculature.

RNA-Sequencing Reveals Activation of Antibody Effector Systems and Mediators of Matrix Organization and Remodeling

Sequencing of ribo-depleted retinal RNA revealed a significant transcriptional dysregulation 6 months after induction of BRB defects, with 6971 transcripts (coding and noncoding) showing 2-fold or higher differential expression. Differentially expressed genes were filtered according to differential expression, expression level, and significance criteria and subjected to gene ontology analysis (Table). Among the upregulated transcripts were multiple mediators of antibody effector systems, including components of the classical complement pathway (C1QA, C1QB, C1QC, and C4B). Complement 3A receptor 1 and the modulator of the complement pathway, SERPING1, were also upregulated. In addition, several transcripts encoding subunits of Fc receptors were increased. Other mediators of immune processes, many of which are known to be expressed in microglia, were overabundant, for example, ADGRE1 (aka F4/80). Markers of lymphoid cells were not expressed (ie, B-cell markers CD79A, CD79B; T-cells markers CD8B1, CD3D, CD3E, CD3G, and T-cell receptor constant or variable gene segments; NK cells markers KLRB1 [aka NK1.1], NCR1, CD27, and IL2RB). Myeloid differentiation marker GR1 (aka LY6G), which is expressed on granulocytes and peripheral neutrophils, and CCR2, a marker for

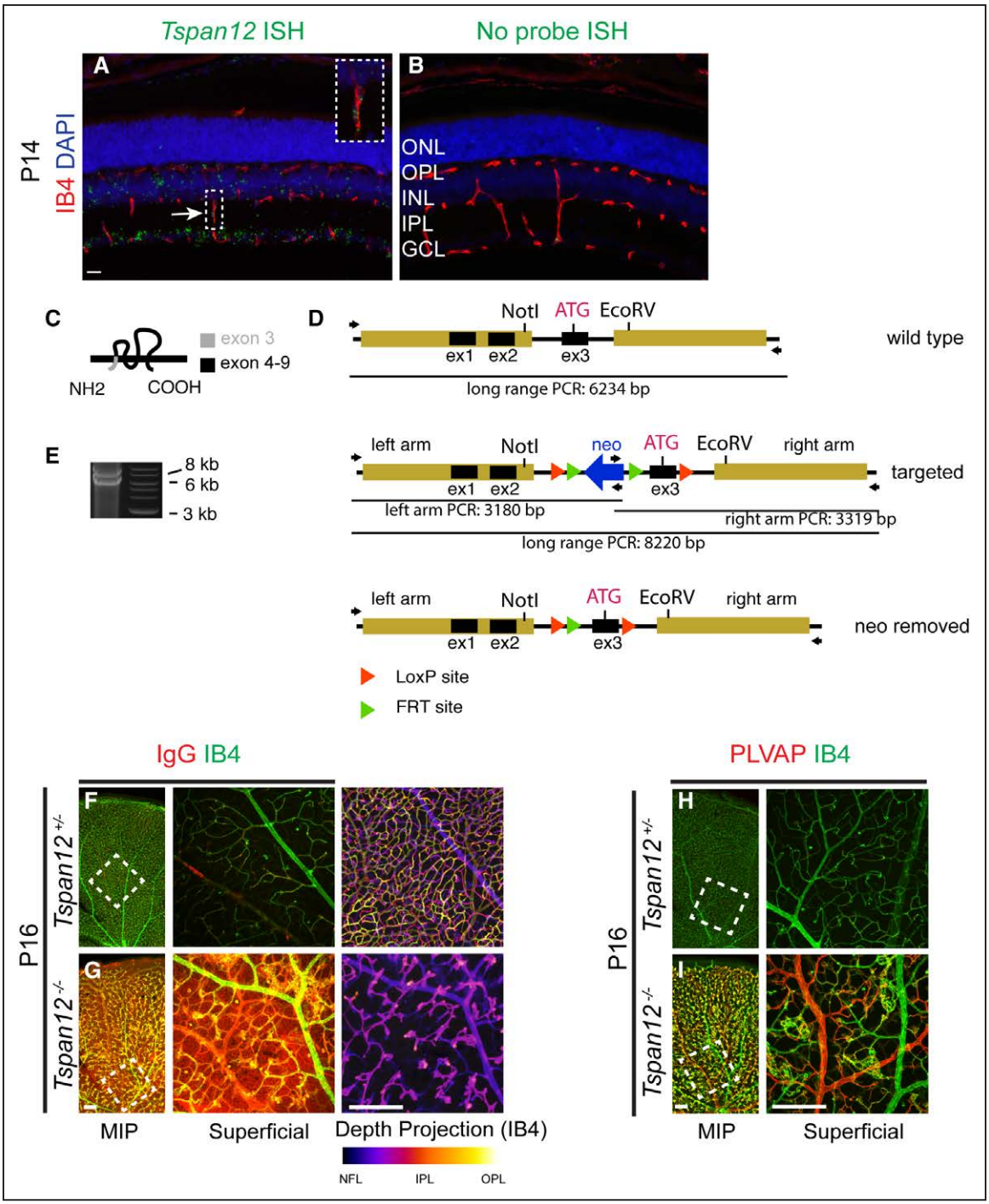

Figure 1. Vascular morphogenesis and blood-retina barrier defects in *Tspan12*$^{-/-}$ mice. **A**, Branched DNA in situ hybridization and amplification with a mTSPAN12 (m tetraspanin 12) probe set, counterstained with isolectinB4 to mark vascular endothelial cells (ECs). Inset highlights a capillary passing through the inner plexiform layer; the m*Tspan12* probe hybridizes to this structure. **B**, Control section processed for signal amplification and detection. **C**, Schematic representation of TSPAN12 protein topology. The start ATG and major portions of the first transmembrane segment are encoded by exon 3. **D**, Schematic representation of the targeting strategy for the generation of the m*Tspan12* LoxP-flanked allele. **E**, Long-range polymerase chain reaction (PCR) yields the expected heterozygous pattern on genomic DNA of the ES cell clone used for blastocyst injection. **F**, IgG is confined to the lumen of blood vessels, and the 3-layered vasculature develops normally in P16 *Tspan12*$^{+/-}$ mice. The **left** shows a maximum intensity projection (MIP) generated from optical sections representing all 3 capillary layers. One petal of a retinal whole mount preparation is shown. An optical section showing the surface blood vessels in the boxed area is shown enlarged and rotated in the **middle**. The **right** shows a color depth projection of all optical sections in the boxed area. **G**, Massive IgG leakage and lack of intraretinal capillaries are observed in *Tspan12*$^{-/-}$ mice. **H** and **I**, Failure to suppress the fenestration component PLVAP (plasmalemma vesicle-associated protein) in ECs of mutant mice. Scale bars **A** and **B**, 20 μm and **F** through **I**, 200 μm. GCL indicates ganglion cell layer; INL, inner nuclear layer; IPL, inner plexiform layer; ONL, outer nuclear layer; and OPL, outer plexiform layer.

blood monocytes, were also not expressed, indicating that leukocytes did not infiltrate the retina at the 6-month time point. However, chemokines, including CCL12 and CXCL10, were strongly upregulated, suggesting activation of microglia. Together, RNA-Seq data revealed involvement of the classical complement pathway as a major consequence of BRB defects.

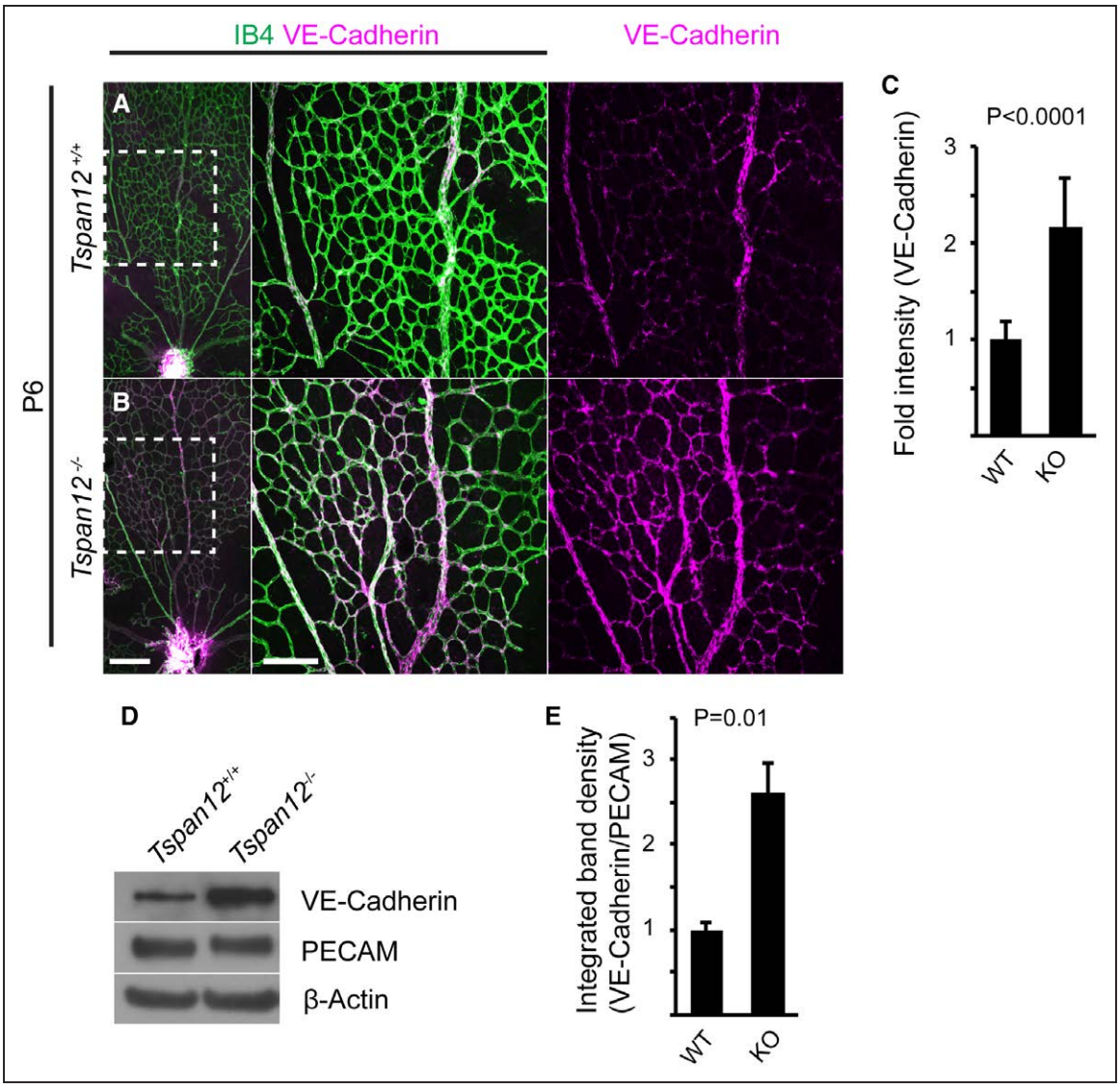

Figure 2. Increased VE-cadherin expression in *Tspan12*$^{-/-}$ retinas. **A** and **B**, Immunostaining of P6 retinal whole mounts reveals increased VE-cadherin expression in *Tspan12*$^{-/-}$ retinal endothelial cells (ECs). **Middle** and **right** show the boxed area enlarged. **C**, Quantification of VE-cadherin staining intensity in n=8 fields of view of 2 retinas per genotype. Data normalized to wild-type (WT) intensity, average+SD shown. **D**, Immunoblot of retinal lysates of the indicated genotype reveals increased VE-cadherin expression. **E**, Quantification of immunoblot band intensity of n=3 P8-10 retinal lysates per genotype. Two retinas of 1 animal were pooled for each lysate. Data normalized to wild-type intensity, average+SD shown. Scale bars: 200 µm. KO indicates knockout; and PECAM, platelet endothelial cell adhesion molecule.

Gene ontology analyses further revealed that transcripts encoding ECM (extracellular matrix) proteins, in particular proteins involved in ECM organization or remodeling of collagen and elastin fibers, were significantly elevated in mutant retinas. MFAPs (microfibrillar-associated proteins) 2 and 4, fibromodulin, fibulin 1, and decorin were in this group (Table). Several of these genes are implicated in vascular basement membrane alterations in DR or diabetic nephropathy (discussion).

Impaired BRB Maintenance Is Associated With Complement Deposition, Cystoid Edema, and Basement Membrane Alterations

Immunostaining of retinal sections from 1-year-old *Tspan12* ECKO revealed that complement component C4, which is essential for the propagation of the classical complement pathway, was strongly increased in multiple foci in and around the inner nuclear layer of *Tspan12* ECKO retinas, indicating localized complement deposition (Figure 5A). Foci of complement deposition were often associated with lesions in the inner nuclear layer and outer plexiform layer. H&E staining of a retinal section (displaying a relatively strongly affected area) showed that the appearance of the lesions is consistent with early stage cystoid edema (Figure 5B). Most cystoid lesions were heavily decorated with IgG and complement. Immunostaining further confirmed increased expression of F4/80 (ADGRE1 in the Table) in microglia, consistent with microglia activation (Figure 5C). Barrier defects resulted in increased extravasation of IgG, transferrin, and albumin (Figure 5D through 5F). Although IgG and albumin extravasation and increased C4 signal were already detectable 1 month after recombination, no lesions were present at early time points (Figure IV in the online-only Data Supplement).

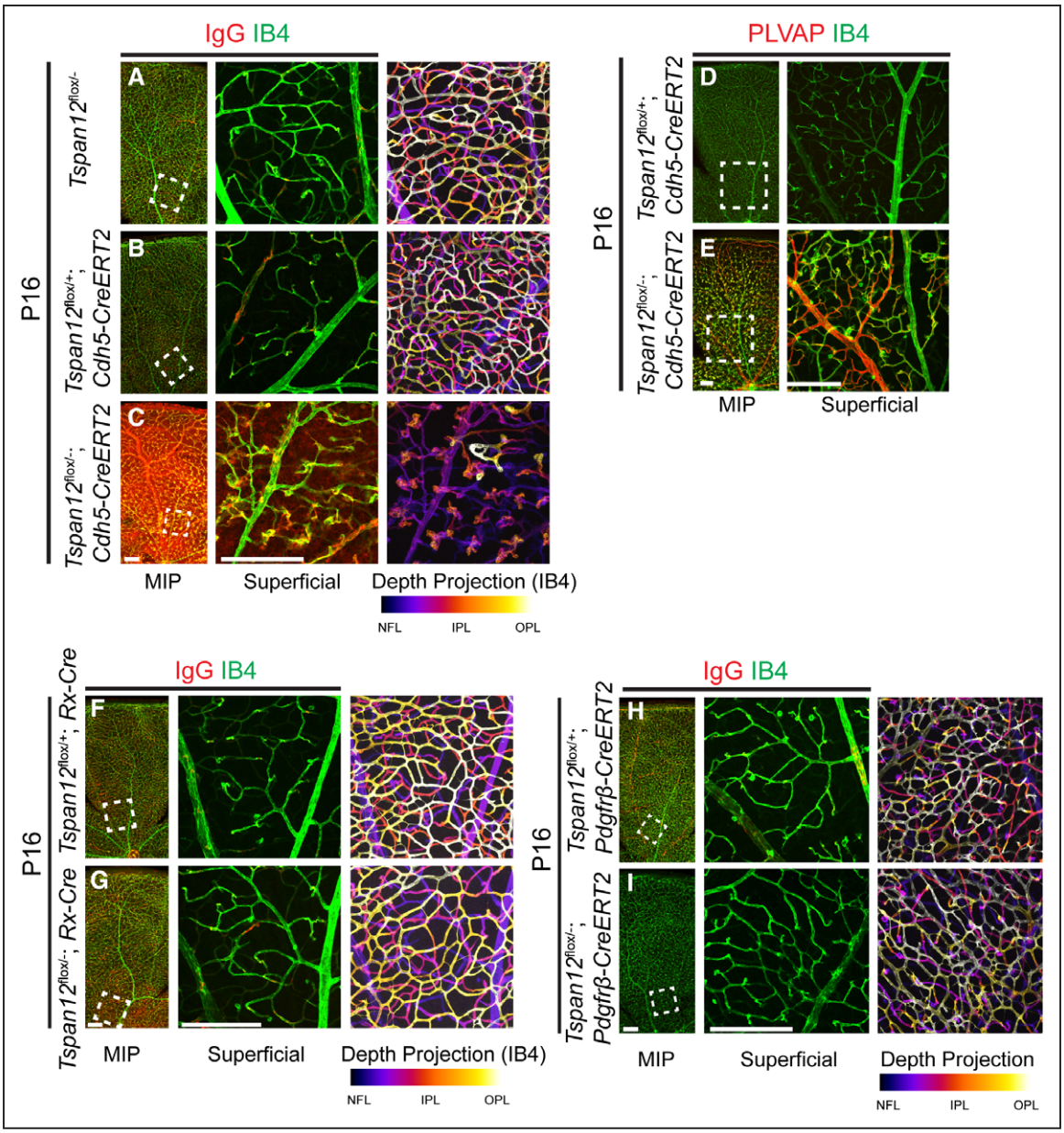

Figure 3. TSPAN12 (tetraspanin 12) functions in retinal vascular endothelial cells (ECs). **A**, Absence of BRB (blood-retina barrier) and vascular morphogenesis defects in *Tspan12*$^{flox/-}$ controls. **B**, *Tspan12*$^{flox/+}$; Cdh5-CreERT2^{+} controls. **C**, IgG and IB4 stains show BRB defects and lack of intraretinal capillaries after inactivation of *Tspan12* in ECs. **D** and **E**, Failure to suppress PLVAP (plasmalemma vesicle-associated protein) in ECs of *Tspan12*$^{flox/-}$; Cdh5-CreERT2^{+} mice. **F** and **G**, Normal BRB and vascular morphogenesis after inactivation of *Tspan12* in retinal precursor cells and in (**H** and **I**) mural cells. Scale bar 200 μm. IPL indicates inner plexiform layer; MIP, maximum intensity projection; and OPL, outer plexiform layer.

Immunostaining also revealed a strongly increased signal for the basement membrane component COL4 surrounding intraretinal capillaries, whereas COL4 staining in the inner limiting membrane of *Tspan12* ECKO retinas was unaltered, providing an internal reference (Figure 5G). In control retinas, vascular COL4 staining was substantially weaker. Genes encoding COL4 chains (COL4A1, COL4A2, COL4A3, COL4A4, COL4A5, and COL4A6) were not among the highly differentially expressed transcripts (0.9- to 1.4-fold change), suggesting that the increased abundance of COL4 in vascular basement membranes could be a consequence of altered matrix remodeling.

Costaining of C4 with IB4, rod-bipolar cell marker PKCα, nuclear Müller cell maker Sox9, microglia marker IBA-1, or with extravasated IgG, showed that C4 partially colocalized with mutant blood vessels, several cell populations of the inner nuclear layer, and microglia. Rod-bipolar cell and Müller glia cell populations appeared disorganized and displayed increased cell spacing (Figure 6). These observations suggest that the function of the inner retina may be impaired.

Reduced b-Wave in Electroretinograms of *Tspan12* ECKO Mice

Electroretinograms were recorded to assess functional consequences of the pathology described in *Tspan12* ECKO mice. Electroretinograms from 8 to 14-month-old, dark-adapted *Tspan12* ECKO mice revealed a similar a-wave (predominantly

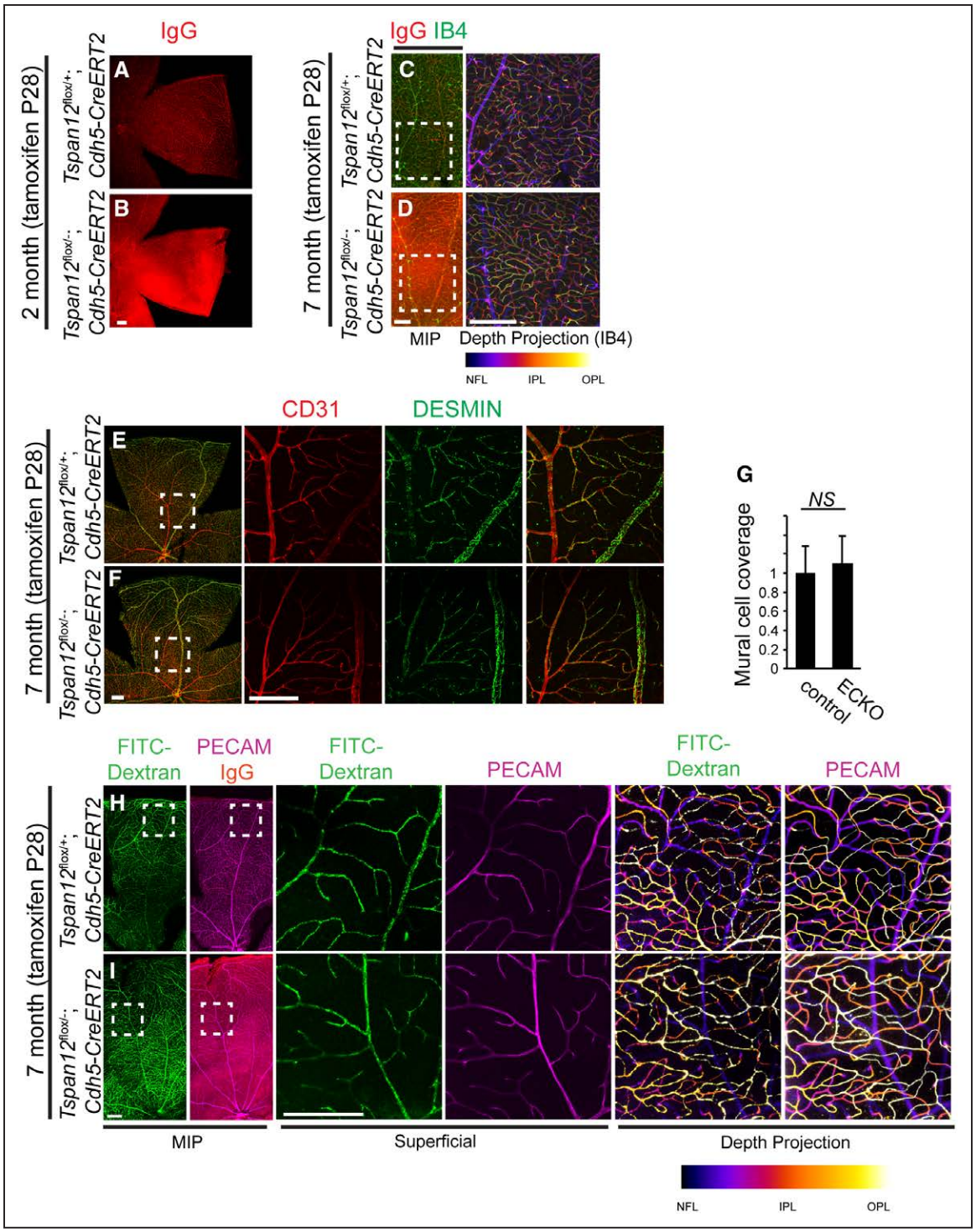

Figure 4. TSPAN12 (tetraspanin 12) is required for BRB (blood-retina barrier) maintenance in an otherwise intact vasculature. **A**, IgG is confined to the lumen of blood vessels in control mice. **B**, IgG leakage 1 mo after endothelial cell (EC)–specific recombination at P28. **C** and **D**, BRB defects in the absence of vascular morphogenesis defects 6 mo after EC-specific recombination at P28. **E** and **F**, Coverage with desmin-positive mural cells is normal in adult *Tspan12* ECKO retinas recombined at juvenile age. **G**, Quantification of mural cell coverage. Sixteen fields of view of 4 retinas per genotype quantified, average+SD shown. **H** and **I**, Transcardial fluorescein isothiocyanate (FITC)-Dextran 500 kDa perfusion and immuno-stain for PECAM (platelet endothelial cell adhesion molecule) and IgG. *Tspan12* ECKO retina shows strong IgG extravasation in an otherwise intact vasculature that is fully perfused. Boxed areas shown enlarged in separate panels. Comparison of depth projections generated from FITC-dextran signal and from PECAM signal shows that the intraretinal capillaries are also fully perfused. Scale bar: 200 μm. IPL indicates inner plexiform layer; MIP, maximum intensity projection; and OPL, outer plexiform layer.

caused by ion currents across photoreceptor membranes) compared with controls. In contrast, we detected a strong reduction of the b-wave (predominantly reflects ion currents across cell membranes in the inner retina) in both dark- and light-adapted *Tspan12* ECKO mice (Figure 7A and 7B). Thus, the reduction of the b-wave and the location of retinal lesions in the inner nuclear layer and outer plexiform layer consistently indicate functional impairment of the inner retina. Together, our data link

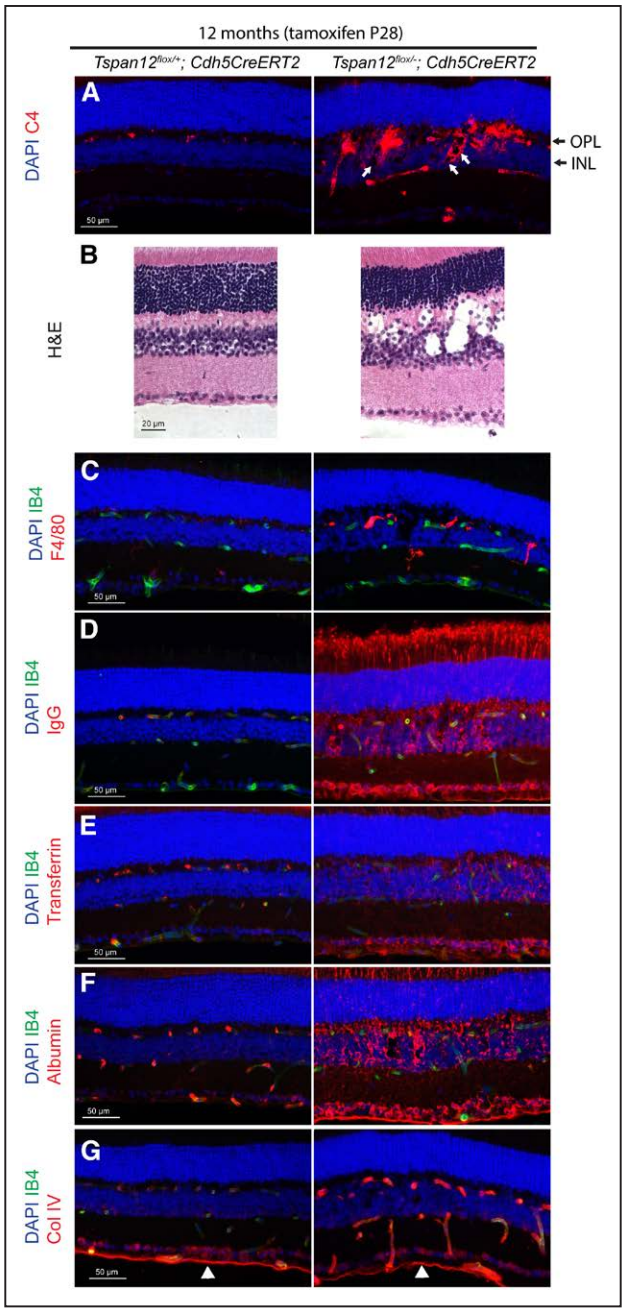

Figure 5. Complement deposition and histopathologic changes in retinas of aged *Tspan12* ECKO mice. **A**, Complement factor C4 deposition around retinal blood vessels, inner nuclear layer (INL), and outer plexiform layer (OPL). White arrows point to some of the small cystoid lesions decorated with complement. **B**, H&E staining of a control retina and a relatively strongly affected area of a mutant retina reveals cystoid lesions consistent with edema. **C**, Increased F4/80 staining on microglia of mutant retinas. **D** through **F**, Extravastion of IgG, transferrin, and albumin in *Tspan12* ECKO retinas. **G**, COL4 (collagen IV) staining in retinal blood vessels of 12-mo-old ECKO mice is increased, staining in the inner limiting membrane (white arrowheads) serves as internal staining control.

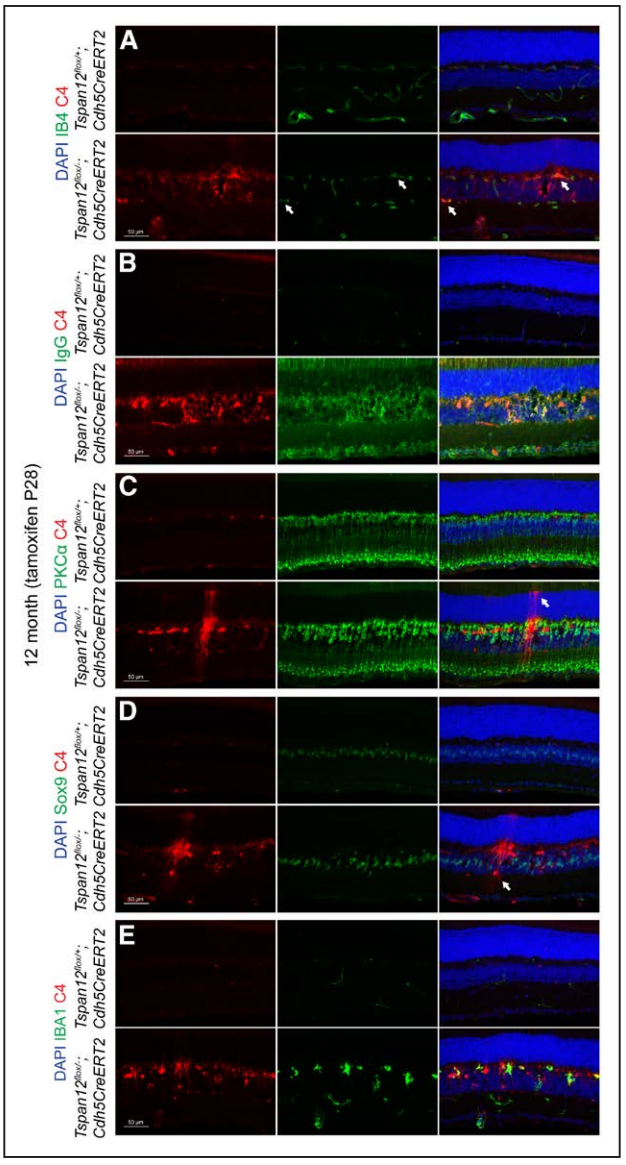

Figure 6. Colocalization of complement factor C4 with several retinal cell types. **A**, Twelve-mo-old *Tspan12* ECKO retinal cross-sections stained with anti-C4 and IB4. Split and merged channels are shown. Arrows indicate blood vessels decorated with C4. **B**, Colocalization of extravasated IgG and C4 on a subset of retinal cells and on the borders of cystoid lesions in the mutant tissue. **C**, Rod-bipolar cell spacing seems increased in the mutant tissue. The section shows also 1 or 2 C4-decorated Müller glia cells, which were recognized by their extensions towards the outer limiting membrane (arrow). **D**, Disorganized Müller cells in the mutant tissue. Sox9 marks nuclei of Müller glia. Arrow highlights a C4-decorated cell which was recognized as amacrine cell based on cell body location and cell shape. **E**, Partial colocalization of C4 with microglia marker IBA-1. PKC indicates protein kinase C; and Sox9, SRY-box 9.

immunoglobulin extravasation, classical complement deposition, cystoid edema, and impaired neuronal function as consequences of an impaired BRB in an otherwise intact vasculature.

Discussion

We previously proposed that TSPAN12 functions as coreceptor in the norrin receptor complex.[14] A prediction of this model is that TSPAN12 functions together with FZD4[15] and LRP5[16] in ECs, which is indeed the case.

CNS angiogenesis requires β-catenin-dependent signaling induced by WNT7A/B or NDP. How canonical signaling enables the vascularization of these CNS tissues is unclear. Interestingly, loss of canonical signaling is associated with a failure of tip cell formation in zebrafish CNS angiogenesis.[43] We find that angiogenesis defects in the retina of *Tspan12* mutant mice correlate with significantly increased VE-cadherin

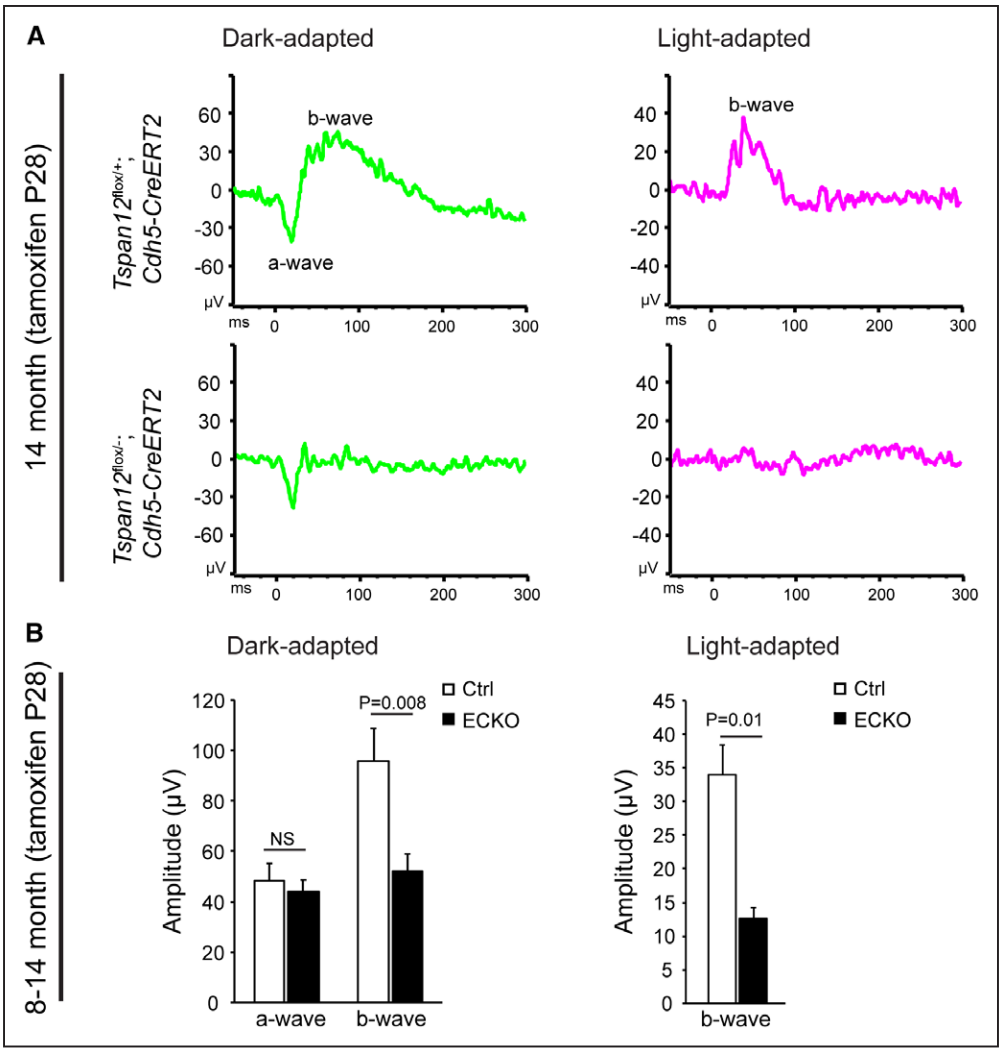

Figure 7. Impaired b-wave in electroretinograms of aged *Tspan12* ECKO mice. **A**, Example of electroretinograms recorded under dark-adapted and light-adapted conditions. **B**, B-wave amplitudes are significantly reduced in *Tspan12* ECKO mice. N=12 (control) or n=6 (ECKO) retinas, average amplitude+SEM shown. Data for light-adapted b-waves were tested for significance using a nonparametric Mann-Whitney U *test*.

expression in ECs. VE-cadherin is a key regulator of EC behavior.[57] Importantly, VE-cadherin suppresses proangiogenic EC behavior—migration and proliferation—in mature blood vessels. Several factors that control EC behavior (eg, VEGF [vascular endothelial growth factor] or S1P [sphingosine-1-phosphate])[58,59] impinge on VE-cadherin by altering its expression, controlling its internalization, or modifying its activity by phosphorylation. Conversely, VE-cadherin is physically associated with receptors, for example, VEGFR2 or TGFβ (transforming growth factor β) receptors, and modulates their activity. Our observation that VE-cadherin protein levels are roughly 2.5-fold increased in ECs of developing *Tspan12* mutant mice suggests that canonical signaling suppresses VE-cadherin, perhaps transiently, to enable migration, proliferation, or tip cell formation. Indeed, EC-specific inactivation of *Cdh5* (ie, VE-cadherin), causes strong hypervascularization of the retina.[59,60] Interestingly, intraretinal capillary formation is especially sensitive to loss of NDP/FZD4 signaling. A reduction of VE-cadherin may be required to reverse the quiescence of the superficial vascular plexus and enable vascularization of intraretinal layers. *Fzd4*$^{-/-}$ EC behavior is normalized by adjacent wild-type cells in genetic mosaics,[26] possibly because mutant cells cannot use increased VE-cadherin levels to fully engage wild-type ECs, which express only normal VE-cadherin levels.

Because TSPAN12 blocking antibodies are under investigation for treating proliferative retinopathies,[61] it is important to consider the roles of TSPAN12 in BRB maintenance. Our genetic studies demonstrate that TSPAN12 is required for BRB maintenance in adult mice.

Among the long-term consequences of BRB defects are cystoid edema and impairment of retinal neural circuit function. These defects are accompanied by inflammation, vascular basement membrane alterations, and increased expression of oxidative stress defense genes (Table). Importantly, BRB impairment, cystoid edema, reduced b-wave and oscillatory potentials, inflammation, basement membrane thickening, and oxidative stress are also among the pathological changes observed in DR,[3,62] implying that BRB defects in an otherwise intact vasculature are sufficient

to recapitulate several key aspects of the DR pathology. Changes of microvascular BM composition and BM thickening are characteristic pathological features of DR[63] and are associated with increased COL4 deposition.[64] Interestingly, the increased COL4 deposition in *Tspan12* ECKO mice is linked to increased expression of several genes involved in ECM organization and remodeling of collagen and elastic fibers. Several of the genes, including MFAP4, fibulin 1, and small proteoglycans decorin and fibromodulin, are also overabundant in DR or diabetic nephropathy.[65–68] Together, *Tspan12* ECKO mice provide a model to untangle the specific pathological consequences of BRB disruption from compounding vascular pathologies observed in pericyte-deficient mice and hyperglycemic animals. Surprisingly, BRB disruption per se is sufficient to recapitulate several characteristics of DR pathology. Furthermore, our findings show how BRB impairment contributes to vision impairment in familial exudative vitreoretinopathy. In a broader view, our findings provide insight into pathological mechanisms downstream of blood-CNS barrier impairment in neurological disease.

Acknowledgments

We thank Dr James Orth in the MCDB light microscopy core facility for assistance in confocal imaging, Micah Stoltz in the animal facility for assistance, the Denver Gene-Targeted Vector Generation, Transgenic and Gene Targeting, and Microarray and Genomics core facilities at the Anschutz Medical Campus in Denver for support, Drs Eric Swindell and Milan Jamrich for providing Rx-Cre mice.

Sources of Funding

This work was supported in part by the Boettcher Foundation Webb-Waring Biomedical Research Award (to H.J. Junge), grants from the National Institutes of Health (EY024261 to H.J. Junge, and EY005856 and EY028147 to J.M. Petrash), and a challenge grant from Research to Prevent Blindness (to Department of Ophthalmology, University of Colorado).

Disclosures

C. Zhang, M.B. Lai, V. Johnson, J.M. Petrash, Z. Chen, and H.J. Junge designed experiments. C. Zhang, M.B. Lai, M.G. Pedler, V. Johnson, and H.J. Junge conducted experiments and analyzed data, R.H. Adams provided unpublished mouse lines. C. Zhang, M.B. Lai, and H.J. Junge wrote the article. All authors edited the article.

References

1. Kempen JH, O'Colmain BJ, Leske MC, Haffner SM, Klein R, Moss SE, Taylor HR, Hamman RF; Eye Diseases Prevalence Research Group. The prevalence of diabetic retinopathy among adults in the United States. *Arch Ophthalmol*. 2004;122:552–563. doi: 10.1001/archopht.122.4.552
2. Cunha-Vaz J, Bernardes R, Lobo C. Blood-retinal barrier. *Eur J Ophthalmol*. 2011;21(suppl 6):S3–S9. doi: 10.5301/EJO.2010.6049
3. Eshaq RS, Aldalati AMZ, Alexander JS, Harris NR. Diabetic retinopathy: breaking the barrier. *Pathophysiology*. 2017;24:229–241. doi: 10.1016/j.pathophys.2017.07.001
4. Gilmour DF. Familial exudative vitreoretinopathy and related retinopathies. *Eye (Lond)*. 2015;29:1–14. doi: 10.1038/eye.2014.70
5. Nikopoulos K, Venselaar H, Collin RW, et al. Overview of the mutation spectrum in familial exudative vitreoretinopathy and Norrie disease with identification of 21 novel variants in FZD4, LRP5, and NDP. *Hum Mutat*. 2010;31:656–666. doi: 10.1002/humu.21250
6. Ye X, Wang Y, Nathans J. The norrin/frizzled4 signaling pathway in retinal vascular development and disease. *Trends Mol Med*. 2010;16:417–425. doi: 10.1016/j.molmed.2010.07.003
7. Nikopoulos K, Gilissen C, Hoischen A, et al. Next-generation sequencing of a 40 Mb linkage interval reveals TSPAN12 mutations in patients with familial exudative vitreoretinopathy. *Am J Hum Genet*. 2010;86:240–247. doi: 10.1016/j.ajhg.2009.12.016
8. Poulter JA, Ali M, Gilmour DF, et al. Mutations in TSPAN12 cause autosomal-dominant familial exudative vitreoretinopathy. *Am J Hum Genet*. 2010;86:248–253. doi: 10.1016/j.ajhg.2010.01.012
9. Charrin S, Jouannet S, Boucheix C, Rubinstein E. Tetraspanins at a glance. *J Cell Sci*. 2014;127(pt 17):3641–3648. doi: 10.1242/jcs.154906
10. van Deventer SJ, Dunlock VE, van Spriel AB. Molecular interactions shaping the tetraspanin web. *Biochem Soc Trans*. 2017;45:741–750. doi: 10.1042/BST20160284
11. Zimmerman B, Kelly B, McMillan BJ, Seegar TCM, Dror RO, Kruse AC, Blacklow SC. Crystal structure of a full-length human tetraspanin reveals a cholesterol-binding pocket. *Cell*. 2016;167:1041.e–1051.e11. doi: 10.1016/j.cell.2016.09.056
12. Junge HJ, Yang S, Burton JB, Paes K, Shu X, French DM, Costa M, Rice DS, Ye W. TSPAN12 regulates retinal vascular development by promoting norrin- but not Wnt-induced FZD4/beta-catenin signaling. *Cell*. 2009;139:299–311. doi: 10.1016/j.cell.2009.07.048
13. Zhang C, Lai MB, Khandan L, Lee LA, Chen Z, Junge HJ. Norrin-induced frizzled4 endocytosis and endo-lysosomal trafficking control retinal angiogenesis and barrier function. *Nat Commun*. 2017;8:16050. doi: 10.1038/ncomms16050
14. Lai MB, Zhang C, Shi J, Johnson V, Khandan L, McVey J, Klymkowsky MW, Chen Z, Junge HJ. TSPAN12 is a norrin co-receptor that amplifies frizzled4 ligand selectivity and signaling. *Cell Rep*. 2017;19:2809–2822. doi: 10.1016/j.celrep.2017.06.004
15. Ye X, Wang Y, Cahill H, Yu M, Badea TC, Smallwood PM, Peachey NS, Nathans J. Norrin, frizzled-4, and Lrp5 signaling in endothelial cells controls a genetic program for retinal vascularization. *Cell*. 2009;139:285–298. doi: 10.1016/j.cell.2009.07.047
16. Huang W, Li Q, Amiry-Moghaddam M, Hokama M, Sardi SH, Nagao M, Warman ML, Olsen BR. Critical endothelial regulation by LRP5 during retinal vascular development. *PLoS One*. 2016;11:e0152833. doi: 10.1371/journal.pone.0152833
17. Chen J, Stahl A, Krah NM, Seaward MR, Dennison RJ, Sapieha P, Hua J, Hatton CJ, Juan AM, Aderman CM, Willett KL, Guerin KI, Mammoto A, Campbell M, Smith LE. Wnt signaling mediates pathological vascular growth in proliferative retinopathy. *Circulation*. 2011;124:1871–1881. doi: 10.1161/CIRCULATIONAHA.111.040337
18. Ohlmann A, Seitz R, Braunger B, Seitz D, Bösl MR, Tamm ER. Norrin promotes vascular regrowth after oxygen-induced retinal vessel loss and suppresses retinopathy in mice. *J Neurosci*. 2010;30:183–193. doi: 10.1523/JNEUROSCI.3210-09.2010
19. Chen Q, Ma JX. Canonical Wnt signaling in diabetic retinopathy. *Vision Res*. 2017;139:47–58. doi: 10.1016/j.visres.2017.02.007
20. Ohlmann A, Tamm ER. Norrin: molecular and functional properties of an angiogenic and neuroprotective growth factor. *Prog Retin Eye Res*. 2012;31:243–257. doi: 10.1016/j.preteyeres.2012.02.002
21. Bassett EA, Tokarew N, Allemano EA, et al. Norrin/frizzled4 signalling in the preneoplastic niche blocks medulloblastoma initiation. *Elife*. 2016;5:e16764. doi: 10.7554/eLife.16764
22. McNeill B, Mazerolle C, Bassett EA, Mears AJ, Ringuette R, Lagali P, Picketts DJ, Paes K, Rice D, Wallace VA. Hedgehog regulates Norrie disease protein to drive neural progenitor self-renewal. *Hum Mol Genet*. 2013;22:1005–1016. doi: 10.1093/hmg/dds505
23. Liebner S, Corada M, Bangsow T, Babbage J, Taddei A, Czupalla CJ, Reis M, Felici A, Wolburg H, Fruttiger M, Taketo MM, von Melchner H, Plate KH, Gerhardt H, Dejana E. Wnt/beta-catenin signaling controls development of the blood-brain barrier. *J Cell Biol*. 2008;183:409–417. doi: 10.1083/jcb.200806024
24. Daneman R, Agalliu D, Zhou L, Kuhnert F, Kuo CJ, Barres BA. Wnt/beta-catenin signaling is required for CNS, but not non-CNS, angiogenesis. *Proc Natl Acad Sci USA*. 2009;106:641–646. doi: 10.1073/pnas.0805165106
25. Stenman JM, Rajagopal J, Carroll TJ, Ishibashi M, McMahon J, McMahon AP. Canonical Wnt signaling regulates organ-specific assembly and differentiation of CNS vasculature. *Science*. 2008;322:1247–1250. doi: 10.1126/science.1164594

26. Wang Y, Rattner A, Zhou Y, Williams J, Smallwood PM, Nathans J. Norrin/frizzled4 signaling in retinal vascular development and blood brain barrier plasticity. *Cell*. 2012;151:1332–1344. doi: 10.1016/j.cell.2012.10.042
27. Zhou Y, Wang Y, Tischfield M, Williams J, Smallwood PM, Rattner A, Taketo MM, Nathans J. Canonical WNT signaling components in vascular development and barrier formation. *J Clin Invest*. 2014;124:3825–3846. doi: 10.1172/JCI76431
28. Chang J, Mancuso MR, Maier C, et al. Gpr124 is essential for blood-brain barrier integrity in central nervous system disease. *Nat Med*. 2017;23:450–460. doi: 10.1038/nm.4309
29. Panagiotou ES, Sanjurjo Soriano C, Poulter JA, et al. Defects in the cell signaling mediator β-catenin cause the retinal vascular condition FEVR. *Am J Hum Genet*. 2017;100:960–968. doi: 10.1016/j.ajhg.2017.05.001
30. Schäfer NF, Luhmann UF, Feil S, Berger W. Differential gene expression in Ndph-knockout mice in retinal development. *Invest Ophthalmol Vis Sci*. 2009;50:906–916. doi: 10.1167/iovs.08-1731
31. Chen J, Stahl A, Krah NM, Seaward MR, Joyal JS, Juan AM, Hatton CJ, Aderman CM, Dennison RJ, Willett KL, Sapieha P, Smith LE. Retinal expression of Wnt-pathway mediated genes in low-density lipoprotein receptor-related protein 5 (Lrp5) knockout mice. *PLoS One*. 2012;7:e30203. doi: 10.1371/journal.pone.0030203
32. Corada M, Orsenigo F, Morini MF, Pitulescu ME, Bhat G, Nyqvist D, Breviario F, Conti V, Briot A, Iruela-Arispe ML, Adams RH, Dejana E. Sox17 is indispensable for acquisition and maintenance of arterial identity. *Nat Commun*. 2013;4:2609. doi: 10.1038/ncomms3609
33. Zhou Y, Williams J, Smallwood PM, Nathans J. Sox7, Sox17, and Sox18 cooperatively regulate vascular development in the mouse retina. *PLoS One*. 2015;10:e0143650. doi: 10.1371/journal.pone.0143650
34. Xu Q, Wang Y, Dabdoub A, Smallwood PM, Williams J, Woods C, Kelley MW, Jiang L, Tasman W, Zhang K, Nathans J. Vascular development in the retina and inner ear: control by norrin and frizzled-4, a high-affinity ligand-receptor pair. *Cell*. 2004;116:883–895.
35. Luhmann UF, Lin J, Acar N, Lammel S, Feil S, Grimm C, Seeliger MW, Hammes HP, Berger W. Role of the Norrie disease pseudoglioma gene in sprouting angiogenesis during development of the retinal vasculature. *Invest Ophthalmol Vis Sci*. 2005;46:3372–3382. doi: 10.1167/iovs.05-0174
36. Kuhnert F, Mancuso MR, Shamloo A, Wang HT, Choksi V, Florek M, Su H, Fruttiger M, Young WL, Heilshorn SC, Kuo CJ. Essential regulation of CNS angiogenesis by the orphan G protein-coupled receptor GPR124. *Science*. 2010;330:985–989. doi: 10.1126/science.1196554
37. Cullen M, Elzarrad MK, Seaman S, et al. GPR124, an orphan G protein-coupled receptor, is required for CNS-specific vascularization and establishment of the blood-brain barrier. *Proc Natl Acad Sci USA*. 2011;108:5759–5764. doi: 10.1073/pnas.1017192108
38. Zhou Y, Nathans J. Gpr124 controls CNS angiogenesis and blood-brain barrier integrity by promoting ligand-specific canonical Wnt signaling. *Dev Cell*. 2014;31:248–256. doi: 10.1016/j.devcel.2014.08.018
39. Posokhova E, Shukla A, Seaman S, Volate S, Hilton MB, Wu B, Morris H, Swing DA, Zhou M, Zudaire E, Rubin JS, St Croix B. GPR124 functions as a WNT7-specific coactivator of canonical β-catenin signaling. *Cell Rep*. 2015;10:123–130. doi: 10.1016/j.celrep.2014.12.020
40. Cho C, Smallwood PM, Nathans J. Reck and Gpr124 are essential receptor cofactors for Wnt7a/Wnt7b-specific signaling in mammalian CNS angiogenesis and blood-brain barrier regulation. *Neuron*. 2017;95:1221–1225. doi: 10.1016/j.neuron.2017.08.032
41. Noda M, Vallon M, Kuo CJ. The Wnt7's tale: a story of an orphan who finds her tie to a famous family. *Cancer Sci*. 2016;107:576–582. doi: 10.1111/cas.12924
42. Ulrich F, Carretero-Ortega J, Menéndez J, et al. Reck enables cerebrovascular development by promoting canonical Wnt signaling. *Development*. 2016;143:147–159. doi: 10.1242/dev.123059
43. Vanhollebeke B, Stone OA, Bostaille N, Cho C, Zhou Y, Maquet E, Gauquier A, Cabochette P, Fukuhara S, Mochizuki N, Nathans J, Stainier DY. Tip cell-specific requirement for an atypical Gpr124- and Reck-dependent Wnt/β-catenin pathway during brain angiogenesis. *Elife*. 2015;4:e06489. doi: 10.7554/eLife.06489
44. Park DY, Lee J, Kim J, Kim K, Hong S, Han S, Kubota Y, Augustin HG, Ding L, Kim JW, Kim H, He Y, Adams RH, Koh GY. Plastic roles of pericytes in the blood-retinal barrier. *Nat Commun*. 2017;8:15296. doi: 10.1038/ncomms15296
45. Ogura S, Kurata K, Hattori Y, et al. Sustained inflammation after pericyte depletion induces irreversible blood-retina barrier breakdown. *JCI Insight*. 2017;2:e90905. doi: 10.1172/jci.insight.90905
46. Enge M, Bjarnegård M, Gerhardt H, Gustafsson E, Kalén M, Asker N, Hammes HP, Shani M, Fässler R, Betsholtz C. Endothelium-specific platelet-derived growth factor-B ablation mimics diabetic retinopathy. *EMBO J*. 2002;21:4307–4316.
47. Hammes HP, Lin J, Renner O, Shani M, Lundqvist A, Betsholtz C, Brownlee M, Deutsch U. Pericytes and the pathogenesis of diabetic retinopathy. *Diabetes*. 2002;51:3107–3112.
48. Bell RD, Winkler EA, Sagare AP, Singh I, LaRue B, Deane R, Zlokovic BV. Pericytes control key neurovascular functions and neuronal phenotype in the adult brain and during brain aging. *Neuron*. 2010;68:409–427. doi: 10.1016/j.neuron.2010.09.043
49. Jiang X, Yang L, Luo Y. Animal models of diabetic retinopathy. *Curr Eye Res*. 2015;40:761–771. doi: 10.3109/02713683.2014.964415
50. Wang Y, Nakayama M, Pitulescu ME, Schmidt TS, Bochenek ML, Sakakibara A, Adams S, Davy A, Deutsch U, Lüthi U, Barberis A, Benjamin LE, Mäkinen T, Nobes CD, Adams RH. Ephrin-B2 controls VEGF-induced angiogenesis and lymphangiogenesis. *Nature*. 2010;465:483–486. doi: 10.1038/nature09002
51. Chen Q, Zhang H, Liu Y, Adams S, Eilken H, Stehling M, Corada M, Dejana E, Zhou B, Adams RH. Endothelial cells are progenitors of cardiac pericytes and vascular smooth muscle cells. *Nat Commun*. 2016;7:12422. doi: 10.1038/ncomms12422
52. Swindell EC, Bailey TJ, Loosli F, Liu C, Amaya-Manzanares F, Mahon KA, Wittbrodt J, Jamrich M. Rx-Cre, a tool for inactivation of gene expression in the developing retina. *Genesis*. 2006;44:361–363. doi: 10.1002/dvg.20225
53. Johnson V, Xiang M, Chen Z, Junge HJ. Neurite mistargeting and inverse order of intraretinal vascular plexus formation precede subretinal vascularization in VLDLR mutant mice. *PLoS One*. 2015;10:e0132013. doi: 10.1371/journal.pone.0132013
54. Itzkovitz S, van Oudenaarden A. Validating transcripts with probes and imaging technology. *Nat Methods*. 2011;8(4 suppl):S12–S19. doi: 10.1038/nmeth.1573
55. Zuercher J, Fritzsche M, Feil S, Mohn L, Berger W. Norrin stimulates cell proliferation in the superficial retinal vascular plexus and is pivotal for the recruitment of mural cells. *Hum Mol Genet*. 2012;21:2619–2630. doi: 10.1093/hmg/dds087
56. Zhao Z, Nelson AR, Betsholtz C, Zlokovic BV. Establishment and dysfunction of the blood-brain barrier. *Cell*. 2015;163:1064–1078. doi: 10.1016/j.cell.2015.10.067
57. Giannotta M, Trani M, Dejana E. VE-cadherin and endothelial adherens junctions: active guardians of vascular integrity. *Dev Cell*. 2013;26:441–454. doi: 10.1016/j.devcel.2013.08.020
58. Gavard J, Gutkind JS. VEGF controls endothelial-cell permeability by promoting the beta-arrestin-dependent endocytosis of VE-cadherin. *Nat Cell Biol*. 2006;8:1223–1234. doi: 10.1038/ncb1486
59. Gaengel K, Niaudet C, Hagikura K, et al. The sphingosine-1-phosphate receptor S1PR1 restricts sprouting angiogenesis by regulating the interplay between VE-cadherin and VEGFR2. *Dev Cell*. 2012;23:587–599. doi: 10.1016/j.devcel.2012.08.005
60. Yamamoto H, Ehling M, Kato K, Kanai K, van Lessen M, Frye M, Zeuschner D, Nakayama M, Vestweber D, Adams RH. Integrin β1 controls VE-cadherin localization and blood vessel stability. *Nat Commun*. 2015;6:6429. doi: 10.1038/ncomms7429
61. Bucher F, Zhang D, Aguilar E, Sakimoto S, Diaz-Aguilar S, Rosenfeld M, Zha Z, Zhang H, Friedlander M, Yea K. Antibody-mediated inhibition of Tspan12 ameliorates vasoproliferative retinopathy through suppression of β-catenin signaling. *Circulation*. 2017;136:180–195. doi: 10.1161/CIRCULATIONAHA.116.025604
62. Klaassen I, Van Noorden CJ, Schlingemann RO. Molecular basis of the inner blood-retinal barrier and its breakdown in diabetic macular edema and other pathological conditions. *Prog Retin Eye Res*. 2013;34:19–48. doi: 10.1016/j.preteyeres.2013.02.001
63. Tsilibary EC. Microvascular basement membranes in diabetes mellitus. *J Pathol*. 2003;200:537–546. doi: 10.1002/path.1439
64. Ban CR, Twigg SM. Fibrosis in diabetes complications: pathogenic mechanisms and circulating and urinary markers. *Vasc Health Risk Manag*. 2008;4:575–596.
65. Blindbæk SL, Schlosser A, Green A, Holmskov U, Sorensen GL, Grauslund J. Association between microfibrillar-associated protein 4 (MFAP4) and micro- and macrovascular complications in

long-term type 1 diabetes mellitus. *Acta Diabetol*. 2017;54:367–372. doi: 10.1007/s00592-016-0953-y
66. Schaefer L, Raslik I, Grone HJ, Schonherr E, Macakova K, Ugorcakova J, Budny S, Schaefer RM, Kresse H. Small proteoglycans in human diabetic nephropathy: discrepancy between glomerular expression and protein accumulation of decorin, biglycan, lumican, and fibromodulin. *FASEB J*. 2001;15:559–561. doi: 10.1096/fj.00-0493fje
67. Cangemi C, Skov V, Poulsen MK, et al. Fibulin-1 is a marker for arterial extracellular matrix alterations in type 2 diabetes. *Clin Chem*. 2011;57:1556–1565. doi: 10.1373/clinchem.2011.162966
68. Freeman WM, Bixler GV, Brucklacher RM, Walsh E, Kimball SR, Jefferson LS, Bronson SK. Transcriptomic comparison of the retina in two mouse models of diabetes. *J Ocul Biol Dis Infor*. 2009;2:202–213. doi: 10.1007/s12177-009-9045-3

Highlights

- Conditional genetics reveal endothelial cell–specific functions of TSPAN12 (tetraspanin 12) in retinal angiogenesis and barriergenesis during development.
- TSPAN12 is required for blood-retina barrier maintenance but is dispensable for vascular maintenance, mural cell coverage, or perfusion in mature mice.
- Late-induced TSPAN12 ECKO mice provide a model to study barrier defects in an otherwise intact vasculature.
- Barrier defects are associated with IgG extravasation, complement deposition, cystoid edema, and reduced electroretinogram b-wave.
- RNA-Seq reveals dysregulation of ECM (extracellular matrix), akin to diabetic retinopathy.